J|A|C|S
ARTICLES
Published on Web 10/26/2002

Nuclear Magnetic Resonance Shifts in Paramagnetic Metalloporphyrins and Metalloproteins

Junhong Mao, Yong Zhang, and Eric Oldfield*

Contribution from the Department of Chemistry, University of Illinois at Urbana-Champaign, 600 South Mathews Avenue, Urbana, Illinois 61801

Received February 26, 2002. Revised Manuscript Received August 21, 2002

Abstract: We report the first detailed investigation of the ^{1}H, ^{13}C, ^{15}N, and ^{19}F nuclear magnetic resonance (NMR) spectroscopic shifts in paramagnetic metalloprotein and metalloporphyrin systems. The >3500 ppm range in experimentally observed hyperfine shifts can be well predicted by using density functional theory (DFT) methods. Using spin-unrestricted methods together with large, locally dense basis sets, we obtain very good correlations between experimental and theoretical results: $R^2 = 0.941$ ($N = 37$, $p < 0.0001$) when using the pure BPW91 functional and $R^2 = 0.981$ ($N = 37$, $p < 0.0001$) when using the hybrid functional, B3LYP. The correlations are even better for C^{α} and C^{β} shifts alone: C^{α}, $R^2 = 0.996$ ($N = 8$, $p < 0.0001$, B3LYP); C^{β}, $R^2 = 0.995$ ($N = 8$, $p < 0.0001$, B3LYP), but are worse for C^{meso}, in part because of the small range in C^{meso} shifts. The results of these theoretical calculations also lead to a revision of previous heme and proximal histidine residue ^{13}C NMR assignments in deoxymyoglobin which are confirmed by new quantitative NMR measurements. Molecular orbital (MO) analyses of the resulting wave functions provide a graphical representation of the spin density distribution in the $[Fe(TPP)(CN)_2]^-$ (TPP = 5,10,15,20-tetraphenylporphyrinato) system ($S = {}^1/_2$), where the spin density is shown to be localized primarily in the d_{xz} (or d_{yz}) orbital, together with an analysis of the frontier MOs in Fe(TPP)Cl ($S = {}^5/_2$), Mn(TPP)Cl ($S = 2$), and a deoxymyoglobin model ($S = 2$). The ability to now begin to predict essentially all heavy atom NMR hyperfine shifts in paramagnetic metalloporphyrins and metalloproteins using quantum chemical methods should open up new areas of research aimed at structure prediction and refinement in paramagnetic systems in much the same way that DFT methods have been used successfully in the past to predict/refine elements of diamagnetic heme protein structures.

Introduction

There has been intense interest in investigating the structures of metalloporphyrins and metalloproteins for many years.[1−4] For metalloporphyrins, X-ray methods give very accurate three-dimensional structural information,[5,6] but X-ray methods are less accurate for the larger protein structures. There is thus interest in using spectroscopic methods to investigate such systems. For example, Mössbauer spectroscopy yields information on the electric field gradient at the Fe nucleus in Fe metalloporphyrins and metalloproteins, and the Mössbauer isomer shift gives information on the charge density at the Fe nucleus.[7] However, these are rather local probes and are not generally available for investigating other metal-containing porphyrins. Here, nuclear magnetic resonance (NMR) spectroscopy can play a role, since essentially every atom in for example a heme protein has one or more NMR active nuclei: ^{1}H, ^{2}H, ^{13}C, ^{14}N, ^{15}N, ^{17}O, and ^{57}Fe, for example, and in some cases, ^{19}F probes may also be utilized.[8] While the quadrupolar nature of some of these nuclei precludes ready detection, ^{1}H, ^{13}C, ^{15}N, ^{19}F, and ^{57}Fe have spin $S = {}^1/_2$, and at least in diamagnetic systems, can be relatively readily detected.

In such diamagnetic systems there are thus numerous potential spectroscopic probes of structure, and we show in Figure 1A a selection of these for a CO heme model system. For this system, we and others have shown previously that it is now possible to compute the ^{13}C isotropic chemical shift, the ^{13}C chemical shift anisotropy, the ^{17}O isotropic chemical shift, the ^{17}O nuclear quadrupole coupling constant, the ^{57}Fe isotropic chemical shift, and the CO infrared stretch frequency,[9] together with as appropriate their perturbations by electrostatic fields,[10] in addition to the ^{57}Fe Mössbauer quadrupole splitting and isomer shift, in this and related systems.[11−14] The ability to connect

* Address correspondence to this author. E-mail: eo@chad.scs.uiuc.edu.

(1) Sanders, L. K.; Arnold, W. D.; Oldfield, E. *J. Porphyrins Phthalocyanines* **2001**, *5*, 323−333.
(2) Bertini, I.; Rosato, A.; Turano, P. *Pure Appl. Chem.* **1999**, *71*, 1717−1725.
(3) Yachandra, V. K. *Methods Enzymol.* **1995**, *246*, 638−675.
(4) Henry, Y.; Ducrocq, C.; Drapier, J. C.; Servent, D.; Pellat, C.; Guissani, A. *Eur. Biophys. J.* **1991**, *20*, 1−15.
(5) Jentzen, W.; Song, X.; Shelnutt, J. A. *J. Phys. Chem. B* **1997**, *101*, 1684−1699.
(6) Salzmann, R.; Ziegler, C. J.; Godbout, N.; McMahon, M. T.; Suslick, K. S.; Oldfield, E. *J. Am. Chem. Soc.* **1998**, *120*, 11323−11334.
(7) Debrunner, P. G. In *Iron Porphyrins*; Lever, A. B. P., Gray, H. B., Eds.; VCH Publishers: New York, 1989; Vol. 3, pp 139−234.
(8) Pearson, J. G.; Montez, B.; Le, H.; Oldfield, E.; Chien, E. Y. T.; Sligar, S. G. *Biochemistry* **1997**, *36*, 3590−3599.
(9) McMahon, M. T.; deDios, A. C.; Godbout, N.; Salzmann, R.; Laws, D. D.; Le, H.; Havlin, R. H.; Oldfield, E. *J. Am. Chem. Soc.* **1998**, *120*, 4784−4797.
(10) deDios, A. C.; Earle, E. M. *J. Phys. Chem. A* **1997**, *101*, 8132−8134.
(11) Grodzicki, M.; Flint, H.; Winkler, H.; Walker, F. A.; Trautwein, A. X. *J. Phys. Chem. A* **1997**, *101*, 4202−4207.

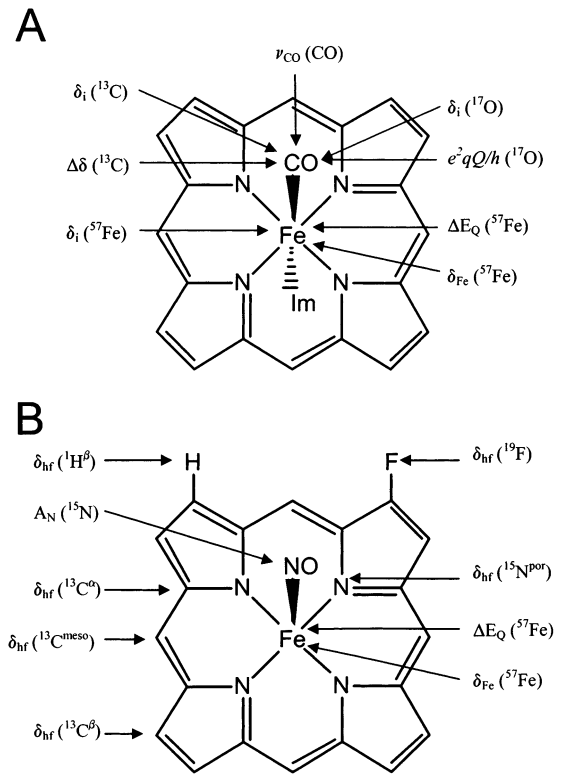

Figure 1. Schematic illustrations of the various spectroscopic probes of structure for metalloporphyrin and metalloprotein model systems: (A) Fe(P)(Im)(CO), diamagnetic; (B) Fe(P)(NO), paramagnetic, $S = {}^1/_2$ (P = porphine). δ_i is the isotropic NMR chemical shift; $\Delta\delta$, NMR chemical shift anisotropy; e^2qQ/h, nuclear quadrupole coupling constant; ΔE_Q, Mössbauer quadrupole splitting; δ_{Fe}, Mössbauer isomer shift; ν_{CO}, CO infrared vibrational stretch frequency; δ_{hf}, NMR hyperfine shift; and A_N, EPR hyperfine coupling constant.

structure with spectroscopy by using modern quantum chemical (density functional theory, DFT) methods then enables the refinement of aspects of protein structure, such as the tilt and bend of the Fe−C−O group in carbonmonoxymyoglobin.[9]

In sharp contrast to these results on diamagnetic systems, there have been no corresponding extensive studies of paramagnetic metalloporphyrins and metalloproteins, in which Fe may exist in many different spin states ($S = {}^1/_2$, 1, ${}^3/_2$, 2, and ${}^5/_2$), even though there are very extensive compilations of both NMR and Mössbauer data for many of these systems. For paramagnetic systems, there are, once again, many spectroscopic observables which might be used in structural studies, and a selection of potential observables for another diatomic-containing metalloporphyrin, a nitrosylmetalloporphyrin, is illustrated in Figure 1B. As with the diamagnetic system, the ^{57}Fe Mössbauer quadrupole splitting and isomer shift are observables, as are the NMR hyperfine shifts for the ^{1}H, ^{13}C, ^{15}N, and ^{19}F nuclei of the porphyrin macrocycle, as well as the axial ligand. In some paramagnetic systems, the axial ligand may also yield NMR observables, while in others, the hyperfine coupling constant (e.g., A_N for an NO) might be measured by electron paramagnetic resonance spectroscopy, and would represent yet another spectroscopic probe. Numerous calculations of hyperfine coupling parameters in small paramagnetic molecules have been reported on the basis of *ab initio*[15−17] and density functional theory methods,[18−23] with the latter appearing to be the most promising ones for handling spin polarization without significant spin contamination. The question then arises: to what extent is it now possible to predict all of these different spectroscopic observables in large paramagnetic systems, by using modern, quantum chemical methods?

To begin to answer this question, we recently investigated the ^{57}Fe Mössbauer quadrupole splittings in a series of diamagnetic as well as paramagnetic metalloprotein and metalloporphyrin systems having $S = 0$, ${}^1/_2$, 1, ${}^3/_2$, 2, and ${}^5/_2$, by using density functional theory, finding excellent correlations between theory and experiment.[24] For example, we predicted the ^{57}Fe Mössbauer quadrupole splitting ΔE_Q with a root-mean-square (rms) error of 0.31 mm sec^{-1} over a 5.63 mm sec^{-1} range ($R^2 = 0.978$, $N = 23$, $p < 0.0001$).[24] This gives some confidence in the quality of the calculations, although the Mössbauer probes are rather local (at the Fe nucleus). We have, therefore, now begun to investigate the NMR hyperfine shifts, which probe the spin distributions throughout the porphyrin macrocycle and, when present, its axial ligands. Importantly, we use the same basic theoretical methods as those used for the Mössbauer quadrupole splittings. This provides a stringent test of the quality of the wave functions obtained, since spectroscopic properties of essentially all atoms are probed, not just a localized subset. In particular, here, we investigate the NMR hyperfine shifts for ^{1}H, ^{13}C, ^{15}N, and ^{19}F in a series of $S = {}^1/_2$, $S = 2$, and $S = {}^5/_2$ metalloporphyrins and metalloproteins, the paramagnetic spin states which are most frequently found in metalloproteins, such as many deoxyhemoglobins, metmyoglobins, and cytochromes. The ability to now predict ΔE_Q as well as many NMR shifts in paramagnetic metalloporphyrins and metalloproteins without use of any empirical methods then gives added confidence to any molecular orbital analyses, as well as providing the possibility of structure refinement, as reported previously for diamagnetic systems.

Experimental Section

Computational Details. Fermi contact spin density calculations were carried out by using density functional theory (DFT) as implemented in Gaussian-98.[25] Spin-unrestricted pure (BPW91[26]) and hybrid (B3LYP[27]) density functionals were employed for all calculations, since these have previously been shown to enable the accurate prediction of ^{57}Fe electric field gradients (Mössbauer quadrupole splittings) in a broad range of both diamagnetic and paramagnetic iron porphyrins, with good accord being found between theory and experiment.[9,12−14,24] And, in addition, the UB3LYP functional has been shown to enable the accurate prediction of ^{57}Fe NMR chemical shifts in diamagnetic metalloproteins,

(12) Godbout, N.; Havlin, R.; Salzmann, R.; Debrunner, P. G.; Oldfield, E. *J. Phys. Chem. A* **1998**, *102*, 2342−2350.
(13) Havlin, R. H.; Godbout, N.; Salzmann, R.; Wojdelski, M.; Arnold, W.; Schulz, C. E.; Oldfield, E. *J. Am. Chem. Soc.* **1998**, *120*, 3144−3151.
(14) Godbout, N.; Sanders, L. K.; Salzmann, R.; Havlin, R. H.; Wojdelski, M.; Oldfield, E. *J. Am. Chem. Soc.* **1999**, *121*, 3829−3844.
(15) Suter, H. U.; Engels, B. *Chem. Phys. Lett.* **1996**, *261*, 644−650.
(16) Maxwell, C. J.; Machado, F. B. C.; Davidson, E. R. *J. Am. Chem. Soc.* **1992**, *114*, 6496−6504.
(17) Chipman, D. M. *J. Chem. Phys.* **1989**, *91*, 5455−5465.
(18) Adamo, C.; Barone, V.; Fortunelli, A. *J. Chem. Phys.* **1995**, *102*, 384−393.
(19) Barone, V.; Adamo, C.; Russo, N. *Chem. Phys. Lett.* **1993**, *212*, 5−11.
(20) Cohen, M. J.; Chong, D. P. *Chem. Phys. Lett.* **1995**, *234*, 405−412.
(21) Eriksson, L. A.; Malkina, O. L.; Malkin, V. G.; Salahub, D. R. *J. Chem. Phys.* **1994**, *100*, 5066−5075.
(22) Lim, M. H.; Worthington, S. E.; Dulles, F. J.; Cramer, C. J. *ACS Symp. Ser.* **1996**, *629*, 402−422.
(23) O'Malley, P. J.; Collins, S. J. *Chem. Phys. Lett.* **1996**, *259*, 296−300.
(24) Zhang, Y.; Mao, J.; Godbout, N.; Oldfield, E. *J. Am. Chem. Soc.* **2002**, *124*, 13921−13930.

metalloporphyrins, and model systems as well as ^{1}H, ^{2}H, and ^{15}N NMR hyperfine shifts in a paramagnetic rubredoxin model system.[28]

For property calculations, we used a Wachters' all electron basis (62111111/3311111/3111) for iron and manganese, 6-311G* for other heavy atoms, and 6-31G* for hydrogen atoms.[29,30] The reasons for using such a "locally dense" scheme[31] are several: First, the metal center is of particular interest from the perspective of spin density determinations; plus, a large number of basis functions are already known to be needed for an accurate description of ^{57}Fe Mössbauer quadrupole splitting and NMR (orbital) shifts.[9,12−14,24,32] Second, since we are primarily interested here in C^{α}, C^{β}, C^{meso} and N^{por} hyperfine shift determinations, we felt that a relatively large porphyrin basis would be desirable. This was found to be the case in initial calculations (data not shown). Third, this locally dense basis approach enables relatively rapid property predictions with no perceptible increase in error over larger basis set calculations. In addition, we also evaluated the Mulliken atomic spin populations and the frontier molecular orbitals. These latter results were displayed by using the Cerius^2 program (Molecular Simulations Inc., San Diego, CA).

Structures Used. We investigated spectroscopic data on the following paramagnetic systems: Fe(TPP)Cl, Mn(TPP)Cl, Mn(TPP)Br, K[Fe(TPP)$(CN)_2$], [Fe(TPP)$(Im)_2$]Cl, and [Fe(TMP)(1-MeIm)$_2$]ClO_4, where TPP = 5,10,15,20-tetraphenylporphyrinato and TMP = 5,10,15,20-tetramesitylporphyrinato. The structures of these systems were obtained from the Cambridge Structural Database (CSD).[33] The reference codes for these porphyrins in the CSD are as follows: KANYUT,[34] TPPMNA01,[35] GISHOF,[35] KCNPFE,[36] FEJDED,[37] and VOFMAE.[38] In addition to these porphyrin systems, we also investigated the heme protein deoxymyoglobin, where we used structures based on those in the Brookhaven Protein Data Bank (PDB; http://www.rcsb.org/pdb/; Files 1A6N[39] and 1BZP[40]).[41] Only the heme moieties were considered. These Fe and Mn porphyrin complexes were chosen to represent the three common paramagnetic spin states: $S = {}^1/_2$, $S = 2$, and $S = {}^5/_2$. As in previous work with both diamagnetic and paramagnetic systems,[12−14,24,32] we truncated these crystal structures by replacing the phenyl groups of TPP, the mesityl groups of TMP, and other peripheral substituents of the heme in deoxymyoglobin with hydrogen atoms, to reduce the computational cost. For [Fe(TPP)$(Im)_2$]Cl and [Fe(TMP)-(1-MeIm)$_2$]ClO_4, there were two molecules in the unit cell and both were investigated. Only the porphyrin moieties (not the counterions) were considered in the calculations. Calculations were performed in this laboratory on Silicon Graphics/Cray Research (Mountain View, CA) 4-processor Origin-200 and 8-processor Origin-300 computers and on SGI Origin-2000 and Power Challenge systems at the National Center for Supercomputing Applications (NCSA) located in Urbana, IL, using up to 16 processors.

Results and Discussion

The observed chemical shift in paramagnetic species can be described as the sum of two terms:

$$\delta_{obs} = \delta_{dia} + \delta_{hf} \tag{1}$$

where δ_{obs}, δ_{dia}, and δ_{hf} are the observed, diamagnetic, and paramagnetic or hyperfine shifts, respectively. δ_{dia} is the shift which would be observed if the molecule contained no unpaired electrons, the conventional orbital or chemical shift, and is generally taken to be the shift value found for a suitable diamagnetic reference compound.[42] The hyperfine shift, δ_{hf}, can itself be divided into two terms:

$$\delta_{hf} = \delta_{con} + \delta_{dip} \tag{2}$$

where δ_{con} is the contact shift and δ_{dip} is the dipolar or pseudocontact shift. The contact shift term arises from spin delocalization from the unpaired electrons, usually located on the metal atom, to the nuclei at the periphery of the molecule through chemical bonds[43] and is directly proportional to the Fermi contact spin density, $\rho_{\alpha\beta}$, at the nucleus of interest:[28,44,45]

$$\delta_{con} = \frac{\mu_0 \mu_B^2 g_e^2 (S+1)}{9kT} \rho_{\alpha\beta} \tag{3}$$

Here, μ_0 is the vacuum permeability ($4\pi \times 10^{-7}$ N A^{-2}), μ_B is the Bohr magneton (9.274×10^{-24} J T^{-1}), g_e is the free electron g-factor, S is the total spin, k is Boltzmann's constant, and T is the absolute temperature. The Fermi contact spin density, $\rho_{\alpha\beta}$, represents the net imbalance between α and β spins at the position of the nucleus of interest. Positive spin density corresponds to a downfield contact shift while negative spin density corresponds to an upfield contact shift. For heavy atoms such as ^{13}C and ^{15}N in metalloporphyrin complexes, the contact shift can be very large, hundreds or thousands of ppm, so consequently it typically overwhelmingly dominates the dipolar

(25) Frisch, M. J.; Trucks, G. W.; Schlegel, H. B.; Scuseria, G. E.; Robb, M. A.; Cheeseman, J. R.; Zakrzewski, V. G.; Montgomery, J. A., Jr.; Stratmann, R. E.; Burant, J. C.; Dapprich, S.; Millam, J. M.; Daniels, A. D.; Kudin, K. N.; Strain, M. C.; Farkas, O.; Tomasi, J.; Barone, V.; Cossi, M.; Cammi, R.; Mennucci, B.; Pomelli, C.; Adamo, C.; Clifford, S.; Ochterski, J.; Petersson, G. A.; Ayala, P. Y.; Cui, Q.; Morokuma, K.; Malick, D. K.; Rabuck, A. D.; Raghavachari, K.; Foresman, J. B.; Cioslowski, J.; Ortiz, J. V.; Baboul, A. G.; Stefanov, B. B.; Liu, G.; Liashenko, A.; Piskorz, P.; Komaromi, I.; Gomperts, R.; Martin, R. L.; Fox, D. J.; Keith, T.; Al-Laham, M. A.; Peng, C. Y.; Nanayakkara, A.; Challacombe, M.; Gill, P. M. W.; Johnson, B.; Chen, W.; Wong, M. W.; Andres, J. L.; Gonzalez, C.; Head-Gordon, M.; Replogle, E. S.; Pople, J. A. *GAUSSIAN 98*, Revision A.9; Gaussian, Inc.: Pittsburgh, PA, 1998.
(26) Becke, A. D. *Phys. Rev. A* **1988**, *38*, 3098−3100. Perdew, J. P.; Wang, Y. *Phys. Rev. B* **1992**, *45*, 13244−13249.
(27) Becke, A. D. *J. Chem. Phys.* **1993**, *98*, 5648−5652. Lee, C.; Yang, W.; Parr, R. G. *Phys. Rev. B* **1988**, *37*, 785−789.
(28) Wilkens, S. J.; Xia, B.; Weinhold, F.; Markley, J. L.; Westler, W. M. *J. Am. Chem. Soc.* **1998**, *120*, 4806−4814.
(29) Wachters, A. J. H. *J. Chem. Phys.* **1970**, *52*, 1033−1036. Wachters, A. J. H. IBM Technol. Report RJ584; 1969.
(30) Basis sets were obtained from the Extensible Computational Chemistry Environment Basis Set Database, Version 1.0, as developed and distributed by the Molecular Science Computing Facility, Environmental and Molecular Sciences Laboratory which is part of the Pacific Northwest Laboratory, P.O. Box 999, Richland, WA 99352, USA and funded by the U.S. Department of Energy. The Pacific Northwest Laboratory is a multiprogram laboratory operated by Battelle Memorial Institute for the U.S. Department of Energy under contract DE-AC06-76RLO 1830. Contact David Feller or Karen Schuchardt for further information.
(31) Chesnut, D. B.; Moore, K. D. *J. Comput. Chem.* **1989**, *10*, 648−659.
(32) Salzmann, R.; McMahon, M. T.; Godbout, N.; Sanders, L. K.; Wojdelski, M.; Oldfield, E. *J. Am. Chem. Soc.* **1999**, *121*, 3818−3828.
(33) Allen, F. H.; Kennard, O. *Chemical Design Automation News* **1993**, *8*(*1*), 1 and 31−37.
(34) Scheidt, W. R.; Finnegan, M. G. *Acta Crystallogr.* **1989**, *C45*, 1214−1216.
(35) Turner, P.; Gunter, M. J.; Skelton, B. W.; White, A. H. *Aust. J. Chem.* **1998**, *51*, 835−851.
(36) Scheidt, W. R.; Haller, K. J.; Hatano, K. *J. Am. Chem. Soc.* **1980**, *102*, 3017−3021.
(37) Scheidt, W. R.; Osvath, S. R.; Lee, Y. L. *J. Am. Chem. Soc.* **1987**, *109*, 1958−1963.
(38) Safo, M. K.; Gupta, G. P.; Walker, F. A.; Scheidt, W. R. *J. Am. Chem. Soc.* **1991**, *113*, 5497−5510.
(39) Vojtěchovský, J.; Chu, K.; Berendzen, J.; Sweet, R. M.; Schlichting, I. *Biophys. J.* **1999**, *77*, 2153−2174.
(40) Kachalova, G. S.; Popov, A. N.; Bartunik, H. D. *Science* **1999**, *284*, 473−476.
(41) Berman, H. M.; Westbrook, J.; Feng, Z.; Gilliland, G.; Bhat, T. N.; Weissig, H.; Shindyalov, I. N.; Bourne, P. E. *Nucleic Acids Res.* **2000**, *28*, 235−242.
(42) Yamamoto, Y. *Annu. Rep. NMR Spectrosc.* **1998**, *36*, 1−77.
(43) Walker, F. A. In *The Porphyrin Handbook*; Kadish, K. M., Smith, K. M., Guilard, R., Eds.; Academic Press: San Diego, CA, 2000; Vol. 5, pp 81−184.
(44) Jesson, J. P. In *NMR of Paramagnetic Molecules, Principles and Applications*; La Mar, G. N., Horrocks, W. D., Jr., Holm, R. H., Eds.; Academic Press: New York, 1973; pp 1−52.
(45) La Mar, G. N. In *NMR of Paramagnetic Molecules, Principles and Applications*; La Mar, G. N., Horrocks, W. D., Jr., Holm, R. H., Eds.; Academic Press: New York, 1973; pp 86−127.

Table 1. Experimental NMR Shift Data, Computed Fermi Contact Spin Densities, and Predicted Hyperfine Shifts for Different Metalloporphyrins/Metalloproteins

							$\rho_{\alpha\beta}$ (au)		predicted δ_{hf}[c] (ppm)	
system	structure model	S	T (K)	site	δ_{obs}[a] (ppm)	δ_{hf}[b] (ppm)	BPW91	B3LYP	BPW91	B3LYP
Fe(TPP)Cl	Fe(TPP)Cl	$^5/_2$	303	C^{α}	1200[46]	1049.2	0.00678	0.00516	1419.7	1123.2
			303	C^{β}	1320[46]	1187.5	0.00530	0.00483	1094.8	1051.4
			303	C^{meso}	500[46]	356.7	−0.00020	0.00049	−111.7	104.5
			293	H^{β}	80[47]	70.8	0.00025	0.00023	−11.0	47.8
Mn(TPP)Cl	Mn(TPP)Cl	2	298	C^{α}	393[48]	242.2	0.00127	0.00134	175.2	251.9
			298	C^{β}	−158[48]	−290.5	−0.00146	−0.00125	−347.3	−241.3
			298	C^{meso}	110[48]	−33.3	−0.00049	−0.00036	−161.1	−71.2
			308	H^{β}		−30.6[d]	−0.00016	−0.00012	−98.4	−25.9
Mn(TPP)Br	Mn(TPP)Br	2	298	C^{α}	398[48]	247.2	0.00158	0.00163	234.1	306.8
			298	C^{β}	−163[48]	−295.5	−0.00132	−0.00113	−320.7	−218.7
			298	C^{meso}	95[48]	−48.3	−0.00054	−0.00044	−170.6	−86.4
Fe((*m*-Me)-TPP)(1,2-diMeIm)	deoxyMb (1A6N)[e]	2	299	C^{α}	1019[49]	868.2	0.00671	0.00488	1210.7	922.9
			299	C^{β}	834[49]	701.5	0.00436	0.00344	762.3	648.9
			299	C^{meso}	125[49]	−18.3	0.00000	0.00004	−68.0	4.4
	deoxyMb (1BZP)[e]	2	299	C^{α}	1019[49]	868.2	0.00727	0.00539	1317.1	1019.3
			299	C^{β}	834[49]	701.5	0.00448	0.00354	785.1	667.8
			299	C^{meso}	125[49]	−18.3	0.00001	0.00014	−66.1	23.3
deoxyMb (3,7-difluoro)	deoxyMb (1A6N)[e]	2	298	F	164.1[50]	233.8	0.00176	0.00141	268.3	265.2
	deoxyMb (1BZP)[e]	2	298	F	164.1[50]	233.8	0.00168	0.00122	253.1	229.3
K[Fe(TPP)$(CN)_2$]	K[Fe(TPP)$(CN)_2$]	$^1/_2$	307	C^{α}	39.8[51]	−111	−0.00110	−0.00080	−170.6	−76.9
			307	C^{β}	90.6[51]	−41.9	−0.00086	−0.00076	−147.8	−73.1
			307	C^{meso}	132.8[51]	−10.5	−0.00033	−0.00041	−98.4	−41.0
			307	H^{β}	−9.9[51]	−19.1	−0.00013	−0.00014	−79.4	−16.4
[Fe(TPP)(1-MeIm)$_2$]Cl	[Fe(TPP)$(Im)_2$]Cl	$^1/_2$	251	C^{α}	13.7[52]	−137.1	−0.00125	−0.00092	−208.6	−107.2
			251	C^{β}	86.6[52]	−45.9	−0.00087	−0.00067	−166.8	−78.8
			251	C^{meso}	37.5[52]	−105.8	−0.00043	−0.00046	−117.4	−54.2
			299	H^{β}		−19.7[f]	−0.00023	−0.00015	−90.8	−18.3
			293	N^{por}		−1660[g]	−0.01606	−0.01990	−1627.9	−1929.1
	[Fe(TMP)(1-MeIm)$_2$]ClO_4	$^1/_2$	251	C^{α}	13.7[52]	−137.1	−0.00127	−0.00096	−212.4	−110.9
			251	C^{β}	86.6[52]	−45.9	−0.00086	−0.00066	−164.9	−76.9
			251	C^{meso}	37.5[52]	−105.8	−0.00037	−0.00041	−109.8	−48.6
			299	H^{β}		−19.7[f]	−0.00022	−0.00015	−88.9	−18.3
			293	N^{por}		−1660[g]	−0.01536	−0.01894	−1561.4	−1836.5
[Fe(TPP)$(Im)_2$]Cl	[Fe(TPP)$(Im)_2$]Cl	$^1/_2$	303	N_1	124.8[53]	−25.7	−0.00121	−0.00105	−182.0	−101.5
			303	N_3	−2115.2[53]	−2346.7	−0.02109	−0.02407	−2047.8	−2256.1
	[Fe(TMP)(1-MeIm)$_2$]ClO_4	$^1/_2$	303	N_1	124.8[53]	−25.7	−0.00082	−0.00051	−144.0	−50.4
			303	N_3	−2115.2[53]	−2346.7	−0.01824	−0.02092	−1783.7	−1961.2

[a] The experimental references for chemical shifts are listed as superscripts. [b] δ_{hf} is obtained by subtracting the diamagnetic shift from the observed chemical shift. Zn(TPP) is used as the diamagnetic reference for the porphyrin carbon and hydrogen atoms, and the shift data are taken from ref 51. For N_1 and N_3 of [Fe(TPP)$(Im)_2$]Cl, the diamagnetic shifts are the values at $T^{-1} \rightarrow 0$ obtained from the Curie plot, from ref 53. For ^{19}F of reconstituted (3,7-difluoro)deoxyMb, the diamagnetic shift is the shift found for the corresponding carbonmonoxyMb, from ref 50, using the average shift of the two ^{19}F signals. [c] Computed from eqs 6 and 7. [d] Fermi contact shift from ref 54. [e] Brookhaven Protein Data Bank accession code for the X-ray structure used in generating the simplified computational model. [f] Fermi contact shift from ref 52. [g] Fermi contact shift from ref 55.

or pseudo-contact shift. As a result, the relationship between the hyperfine shift and the Fermi contact spin density can be expressed in a simplified form:

$$\delta_{hf} \approx \delta_{con} = m\frac{S+1}{T}\rho_{\alpha\beta} \tag{4}$$

where m is a collection of physical constants:

$$m = \frac{\mu_0 \mu_B^2 g_e^2}{9k} = 23.5 \times 10^6 \text{ ppm K au}^{-1} \tag{5}$$

To test to what extent the ^1H, ^{13}C, ^{15}N, and ^{19}F NMR hyperfine shifts can be predicted in paramagnetic metalloporphyrins and metalloproteins using this approach, we therefore evaluated $\rho_{\alpha\beta}$ for the systems described above, which cover all common paramagnetic spin states. Table 1 summarizes the experimental chemical shifts,[46−53] hyperfine shifts,[50−55] computed Fermi contact spin densities, and predicted hyperfine shifts for these systems. There are eight C^{α}, eight C^{β}, four C^{meso}, eight H^{β}, and four N^{por} atoms in each porphyrin ring. And, for the porphyrin-imidazole complexes, additional results are available for the axially coordinated imidazole ring, shown below with its numbering system:

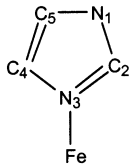

The average values of the spin densities for each type of atom are given in Table 1. These results are shown graphically in

(46) Goff, H. M.; Shimomura, E. T.; Phillippi, M. A. *Inorg. Chem.* **1983**, *22*, 66−71.
(47) Wojaczyński, J.; Latos-Grażyński, L.; Hrycyk, W.; Pacholska, E.; Rachlewicz, K.; Szterenberg, L. *Inorg. Chem.* **1996**, *35*, 6861−6872.
(48) Turner, P.; Gunter, M. J. *Inorg. Chem.* **1994**, *33*, 1406−1415.
(49) Shirazi, A.; Leum, E.; Goff, H. M. *Inorg. Chem.* **1983**, *22*, 360−362.
(50) Yamamoto, Y.; Hirai, Y.; Suzuki, A. *JBIC, J. Biol. Inorg. Chem.* **2000**, *5*, 455−462.
(51) Wüthrich, K.; Baumann, R. *Helv. Chim. Acta* **1973**, *56*, 585−596.
(52) Goff, H. M. *J. Am. Chem. Soc.* **1981**, *103*, 3714−3722.
(53) Yamamoto, Y.; Nanai, N.; Inoue, Y.; Chûjô, R. *J. Chem. Soc., Chem. Commun.* **1989**, 1419−1421.
(54) La Mar, G. N.; Walker, F. A. *J. Am. Chem. Soc.* **1975**, *97*, 5103−5107.
(55) Goldammer, E. v. *Z. Naturforsch.* **1979**, *34C*, 1106−1111.

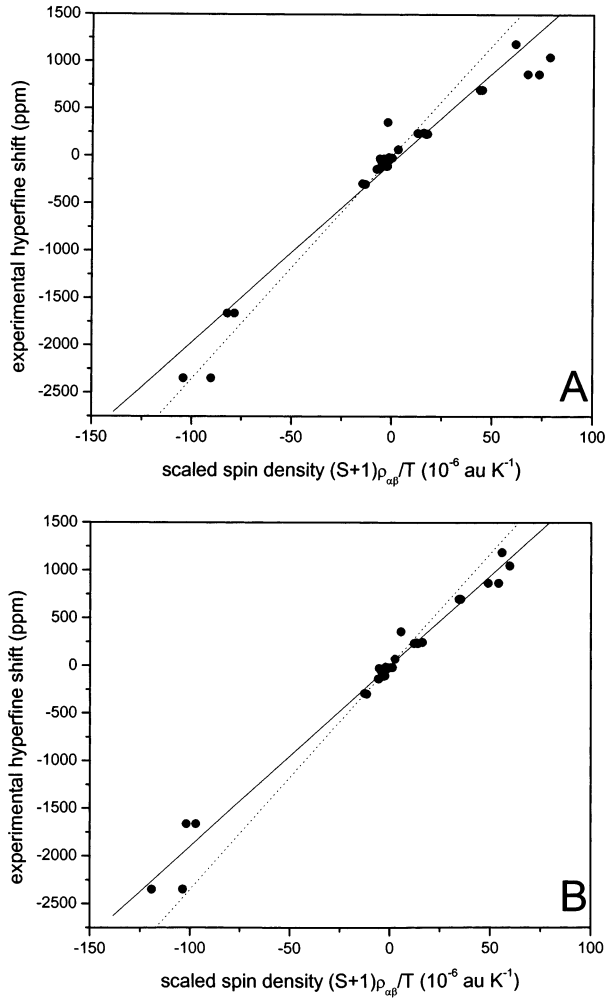

Figure 2. Graph showing experimental NMR hyperfine shifts versus thermal and spin scaled Fermi contact spin densities computed via DFT methods: (A) BPW91 functional, slope = 19.0, $R^2 = 0.941$; (B) B3LYP functional, slope = 18.9, $R^2 = 0.981$. The solid lines indicate the best linear fits of the data, while the dotted lines represent the ideal theoretical lines with a slope of 23.5 and a *y*-intercept of 0.

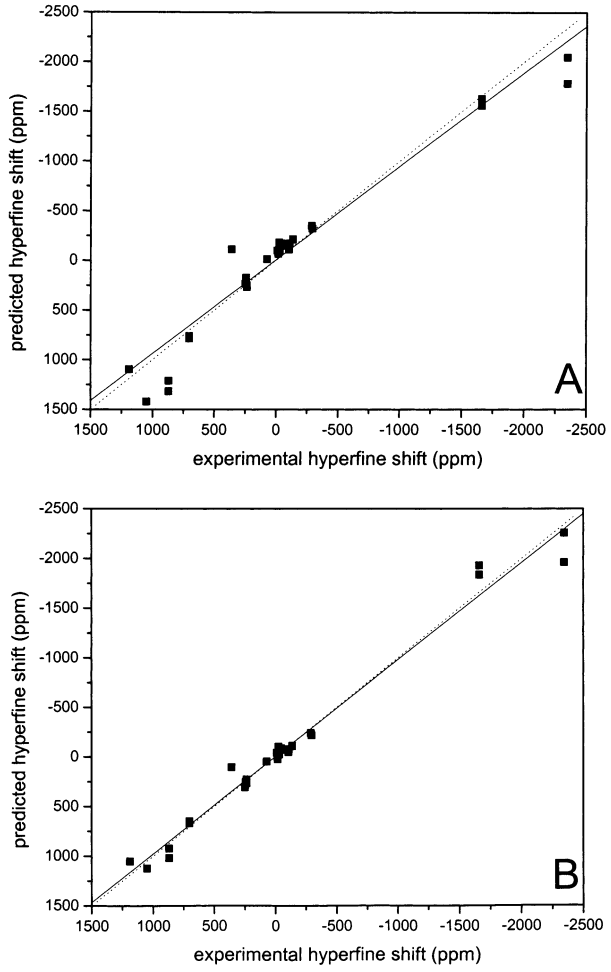

Figure 3. Graph showing experimental NMR hyperfine shifts plotted versus predicted hyperfine shifts computed by using DFT methods and eqs 6 and 7: (A) BPW91 functional, $R^2 = 0.941$, SD = 186 ppm; (B) B3LYP functional, $R^2 = 0.981$, SD = 108 ppm. The dotted lines are drawn for comparison with unit slope, passing through the origin.

Figure 2, where we present linear regression fits of the experimental hyperfine shifts versus the scaled Fermi contact spin densities, $(S + 1)\rho_{\alpha\beta}/T$, computed by using the BPW91 (Figure 2A) and B3LYP (Figure 2B) functionals. The solid lines represent the best fits of the data points, while the dotted lines correspond to the theoretical lines with the ideal slope 23.5. There is clearly a very good correlation between the experimental hyperfine shifts and the scaled spin densities in both cases. For the BPW91 functional results, Figure 2A, the slope of the correlation line for all 37 points is 19.0, the R^2 value is 0.941 ($p < 0.0001$), and the intercept is −68.0 ppm. This improves in the case of the B3LYP results, Figure 2B. Here, we find a slope of 18.9, an R^2 value of 0.981 ($p < 0.0001$), and an intercept of only −3.2 ppm. These results can be fitted by using the following two equations:

$$\delta_{\mathrm{hf}}(\mathrm{BPW91}) = 19.0 \times 10^6\left(\frac{S+1}{T}\rho_{\alpha\beta}\right) - 68.0 \qquad (6)$$

$$\delta_{\mathrm{hf}}(\mathrm{B3LYP}) = 18.9 \times 10^6\left(\frac{S+1}{T}\rho_{\alpha\beta}\right) - 3.2 \qquad (7)$$

For more ready comparison with experiment, we show in Figure 3 the experimental hyperfine shifts plotted versus the predicted hyperfine shifts, derived from eqs 6 and 7. The *x*-axis scale is that which corresponds to the conventional δ scale for chemical shifts, with high-frequency, low-field, paramagnetic or deshielded values being more positive. In each of the graphs, the solid correlation line is very close to the ideal 45° line (the dotted line). Root-mean-square deviations of 186 and 108 ppm over a total shift range of 3500 ppm are obtained for the BPW91 (Figure 3A) and B3LYP (Figure 3B) results, respectively. These results strongly suggest that the contact shift dominates the hyperfine shift at least for the heavy atoms in these systems (which dominate the overall "chemical" shift range), and there is clearly good agreement between the theoretical predictions and experimental results.

One puzzling feature of our results, however, concerns deoxymyoglobin. In Table 1 and Figure 2, we used the solution NMR shifts for Fe((*m*-Me)-TPP)(1,2-diMeIm),[49] finding good accord between theory and experiment. Interestingly, however, Yamamoto and Chûjô have reported the heme and proximal histidine shifts in deoxymyoglobin itself,[56] but their assignment of the C^{α}, C^{β} shifts to the 780−840 ppm range may be in error. Specifically, they suggested that the peaks in this region correspond to 16 carbons, but on integration of their experi-

(56) Yamamoto, Y.; Chûjô, R. *J. Chem. Soc., Chem. Commun.* **1992**, 87−89.

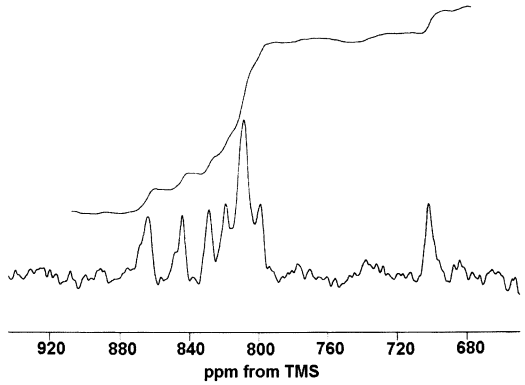

Figure 4. 90.5 MHz ^{13}C NMR spectrum of horse heart deoxymyoglobin at 23 °C. Peaks in the 800−865 ppm range correspond to eight carbon atoms and are assigned to C^{β}.

Table 2. Experimental ^{13}C NMR Chemical Shifts, Hyperfine Shifts, Assignments, and Predictions for Deoxymyoglobin

experimental shift (ppm)[a]	assignment[b]	diamagnetic shift (ppm)[c,d]	hyperfine shift (ppm)[a]	predicted hyperfine shift (ppm) 1A6N[e]	1BZP[f]
800−865 (780−840)	C^{β}	132.5	700 (677.5)	630	649
700.4 (686.3)	C_5	119.0	581.4 (567.3)	430	441
234.7 (235.3)	C_2	132.1	102.6 (103.2)	19	78

[a] The shifts shown are from this work; those in parentheses are from ref 56. [b] The assignments shown are those made in this work. [c] C_2 and C_5 diamagnetic reference shifts are for $[Co(TPP)(1\text{-}MeIm)_2]Cl$ at 26 °C, from ref 52. [d] The C^{β} reference is Zn(TPP) at 34 °C, ref 51. [e] Brookhaven Protein Data Bank file 1A6N (ref 39). [f] Brookhaven Protein Data Bank file 1BZP (ref 40).

mental spectrum, we find that they correspond to only ∼8 carbons (using their single carbon "C_2" and "C_4" peaks as "internal standards"). To investigate this point in more detail, we therefore repeated their measurements at higher field and at a variety of recycle times and we obtained the spectrum shown in Figure 4. The intensity at 800−865 ppm clearly corresponds to 8 not 16 carbons and was independent of recycle time. These results, together with our theoretical calculations, strongly suggest that in deoxymyoglobin only the less shifted C^{β} carbons are being observed, with C^{α} being unobservable because of increased line widths. A search for C^{α} in the predicted shift range (1050−1400 ppm) was unsuccessful. Since the peak at 686.3 ppm does not split into a doublet in a ^1H-coupled spectrum while that at 235.3 ppm does,[56] it also seems likely that the 686.3 ppm peak comes from C_5 of the proximal histidine, while that at 235.3 ppm is due to either C_2 or C_4, which are both protonated.

The results of our quantum chemical calculations also support the need for a spectral reassignment. For example, we show in Table 2 the experimentally observed ^{13}C NMR shifts for the peaks in question together with our proposed assignments, the diamagnetic reference shifts, the experimental hyperfine shifts, and the hyperfine shifts computed by using the B3LYP functional (eq 7). We investigated structures based on both the 1A6N and 1BZP X-ray crystal structures. As can be seen in Table 2, there is generally good agreement with the assignments proposed: C^{β} shifts are mostly downfield, 800−865 ppm from experiment or an average hyperfine shift of ∼700 ppm, in good accord with the 630, 649 ppm hyperfine shifts computed by using the 1A6N or 1BZP geometries. The peak at 700.4 ppm is attributed to C_5 on the basis of its hyperfine shift (581.4 ppm

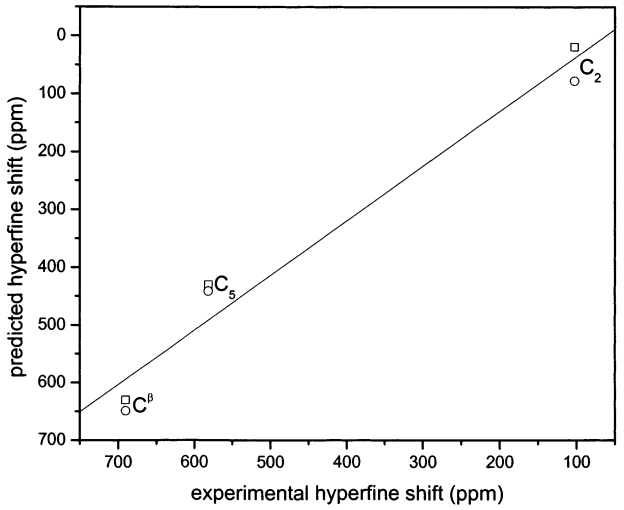

Figure 5. Graph showing correlation between the experimental and computed hyperfine shifts for C^{β}, C_5, and C_2 in horse deoxymyoglobin. DFT calculations using the B3LYP hybrid XC functional based on porphine structures extracted from PDB Files 1A6N (□) and 1BZP (○) (refs 39, 40). $R^2 = 0.965$, slope = 0.95.

experimental; 430, 441 ppm computed) together with the fact that it is not a doublet in the coupled spectrum, and the feature at 234.7 ppm is reassigned to C_2 on the basis of its doublet splitting and small experimental and computed hyperfine shifts. On the other hand, C_4 is not detected, since it is predicted to have an observed shift of about −10 ppm from TMS and would, thus, likely be obscured by the protein envelope. These results are shown graphically in Figure 5, where we present results based on both deoxymyoglobin structures. Using data for both structures, we find an overall $R^2 = 0.965$ and a slope of 0.95 for C^{β}, C_5, and C_2, supporting the assignments proposed. The lack of observation of C^{α} peaks may at first appear surprising, however, in deoxyhemoglobin, none of the C^{α}, C^{β}, or C_5 peaks are observable,[56] even at high field (data not shown), indicating very rapid T_2 relaxation.

Incorporation of the C^{β}, C_5, and C_2 results into the previous correlations causes only a small change in the statistics: for BPW91, we find a slope = 18.9, $R^2 = 0.943$, SD = 182 ppm ($N = 43$, $p < 0.0001$), and for B3LYP, we find a slope = 19.1, $R^2 = 0.981$, SD = 106 ppm ($N = 43$, $p < 0.0001$). These results indicate that the B3LYP calculations provide both a slightly better R^2 value (0.981 versus 0.943) as well as a smaller rms deviation (106 versus 182 ppm), consistent with the better performance of B3LYP in computing the ^{57}Fe Mössbauer and NMR properties reported previously.[12] What, then, are the major contributors to the errors in the predictions? First, there might be structural uncertainties. However, these effects would most likely contribute to the R^2 values (which are already good) and not to systematic errors in the slopes, which are about 20% lower that predicted by eqs 4 and 5. Thus, basis/functional or other methodological deficiencies (such as use of Gaussian vs Slater/numerical basis sets) appear to contribute in a systematic way, causing the slope to deviate from its theoretical value, although no obvious improvements were obtained when numerical basis/STO calculations using the Amsterdam Density Functional (ADF) code[57] were employed. These effects can be clearly seen

(57) ADF 2000.02. http://www.scm.com, Vrije Universiteit, Theoretical Chemistry, Amsterdam, The Netherlands.

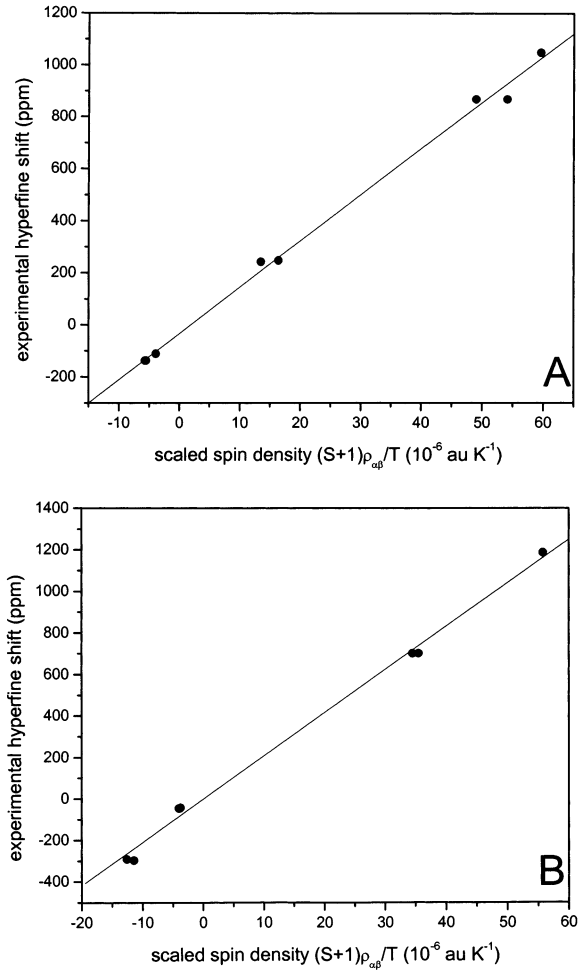

Figure 6. Graph showing correlation between experimental C^{α} and C^{β} hyperfine shifts and the scaled Fermi contact spin densities computed via the DFT/B3LYP method. (A) C^{α} ($N = 8$, slope = 17.8, $R^2 = 0.996$); (B) C^{β} ($N = 8$, slope = 20.9, $R^2 = 0.995$).

when the overall data are broken down into smaller subsets. For example, the B3LYP results for C^{α} and C^{β} both yield very high correlation coefficients (C^{α}, $R^2 = 0.996$, $N = 8$; C^{β}, $R^2 = 0.995$, $N = 8$), as shown in Figure 6A and B, but the slopes of the two correlations are rather different: 17.8 for C^{α} and 20.9 for C^{β}. When both C^{α} and C^{β} data points are incorporated into one correlation, the R^2 value degrades to 0.983 ($N = 16$, $p < 0.0001$) and the slope changes to 18.9. In addition, there are also expected to be some errors due to the truncation of peripheral metalloporphyrin substituents, such as phenyl and mesityl groups, necessary to make the calculations computationally tractable. The effects are expected to be most important for the C^{meso} shift calculations, since we are concerned, primarily, with meso-substitutions. Moreover, since the C^{meso} shift range is much smaller than that of C^{α} or C^{β} (500 ppm for C^{meso} versus 1200 ppm for C^{α} and 1500 ppm for C^{β}), C^{meso} shift calculations are expected to be the least accurate, and indeed, we find $R^2 = 0.717$ for the meso-carbons investigated. However, since the experimental C^{meso} shift range is relatively small, due to a small spin delocalization towards these positions, the contribution of the C^{meso} data to the overall correlation is likewise small and removal of C^{meso} data points does not improve the correlation significantly.

Electronic Structures

Low-Spin Fe(III) ($S = {}^1/_2$) Porphyrins. We next investigated the electronic structures of the three six-coordinate low-spin ($S = {}^1/_2$) ferric porphyrin complexes: $[Fe(TPP)(CN)_2]^-$, $[Fe(TPP)(Im)_2]^+$, and $[Fe(TMP)(1\text{-}MeIm)_2]^+$. These all have a highly planar porphyrin ring and a common ground state with a $(d_{xy})^2(d_{xz}d_{yz})^3$ electron configuration.[58] For $[Fe(TPP)(CN)_2]^-$, the frontier molecular orbital analyses indicate that the α-spin d_{xz}, d_{xy}, and d_{yz} are all occupied, while for the β-spins, d_{xz} (or d_{yz}) and d_{xy} are occupied, which corresponds to $(d_{xy})^2(d_{xz}d_{yz})^3$, clearly the same picture as a conventional ligand field description. Moreover, it is known that the β-LUMO orbital in $S = {}^1/_2$ systems reflects the excess α-electron density.[59] This can be seen in Figure 7 by comparison of the contour plots of the β-LUMO (Figure 7A) and the positive spin density (Figure 7B) for $[Fe(TPP)(CN)_2]^-$. Clearly, most of the spin density is localized in the d_{xz}/d_{yz} molecular orbital. These results are generally very similar to those we have recently found for $[Fe(TMP)(1\text{-}MeIm)_2]^+$.[24]

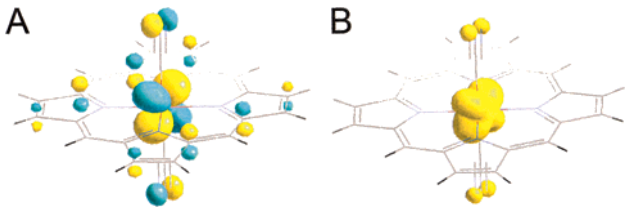

Figure 7. (A) β-LUMO and (B) positive spin density for $[Fe(TPP)(CN)_2]^-$ (contour values = ±0.05 and 0.005 au, respectively).

In the case of $[Fe(TPP)(Im)_2]^+$ and $[Fe(TMP)(1\text{-}MeIm)_2]^+$, there are two molecules in each unit cell. For each of these four molecules, the porphyrin ring is again essentially planar and the ligands align in an antiparallel fashion. The two molecules in the same unit cell have different $Fe-N^{por}$ and $Fe-N_3$ bond lengths and different ligand orientations, Table 3, but the structures of the corresponding molecules of $[Fe(TPP)(Im)_2]^+$ and $[Fe(TMP)(1\text{-}MeIm)_2]^+$ (models 1 and 3, models 2 and 4 in Table 3) are very similar. As expected, the results of the spin density calculations on the corresponding models reflect this similarity, with R^2 values of 0.996 and 1.000 being obtained for models 1 versus 3 and 2 versus 4, respectively. The methyl groups in the 1-methylimidazole ligands, thus, have little influence on the spin density distributions in the porphyrin ring or on the ligands. We therefore analyze just the results for $[Fe(TPP)(Im)_2]^+$. On the basis of our DFT calculations, the energy of model 1 is lower than that of model 2 (by 0.32 eV, BPW91; 0.37 eV, B3LYP), indicating that model 1 is more stable. This is also reflected in the structures. In model 1, the two imidazole ligands are aligned approximately along one $N^{por}-Fe-N^{por}$ axis and the two $Fe-N^{por}$ bonds along this axis are longer than the other two $Fe-N^{por}$ bonds. In model 2, the two imidazole ligands are aligned along one $C^{meso}-Fe-C^{meso}$ axis. In addition, model 2 has shorter $Fe-N_3$ bonds than those of model 1. These structural differences lead to greater steric repulsion between the ligands and the porphyrin ring in model

(58) Nakamura, M.; Ikeue, T.; Ikezaki, A.; Ohgo, Y.; Fujii, H. *Inorg. Chem.* **1999**, *38*, 3857−3862.
(59) George, S. D.; Metz, M.; Szilagyi, R. K.; Wang, H.; Cramer, S. P.; Lu, Y.; Tolman, W. B.; Hedman, B.; Hodgson, K. O.; Solomon, E. I. *J. Am. Chem. Soc.* **2001**, *123*, 5757−5767.

Table 3. Comparison of Selected Structural Parameters and Computed Energies for Both Molecules in the Unit Cells of $[Fe(TPP)(Im)_2]^+$ and $[Fe(TMP)(1\text{-}MeIm)_2]^+$

model	system	d(Fe–N^{por})[a] (Å)	d(Fe–N$_3$) (Å)	θ[b] (deg)	E[c] (au) BPW91	E[c] (au) B3LYP
1	$[Fe(TPP)(Im)_2]^+$	1.986, 2.002	1.977	6	−2704.4495	−2704.4853
2	$[Fe(TPP)(Im)_2]^+$	1.992	1.964	42	−2704.4376	−2704.4716
3	$[Fe(TMP)(1\text{-}MeIm)_2]^+$	1.974, 2.002	1.975	23	−2782.9126	−2782.9742
4	$[Fe(TMP)(1\text{-}MeIm)_2]^+$	1.987	1.964	42	−2782.8902	−2782.9522

[a] Single entries represent the mean values over four Fe−N^{por} bond lengths. Dual entries are those along orthogonal axes. [b] Dihedral angle between the imidazole plane and the N^{por}−Fe−N^{por} axis. [c] Energy computed using the locally dense basis/DFT methods described in the text.

2. The thermodynamically most stable position for the two parallel imidazole ligands is to align along the N^{por}−Fe−N^{por} axis.[60] Although in solution the ligands may rotate or jump about the Fe−N$_3$ bond axis, they can be expected to be located primarily along the N^{por}−Fe−N^{por} axes. Fermi contact spin density results for both models 1 and 2 (data not shown) are in good accord with the experimental hyperfine shifts. When compared with the other complexes investigated, model 1 of $[Fe(TPP)(Im)_2]^+$ gives a large asymmetric spin distribution on the porphyrin carbons. This can be explained by the locations of the axial ligands along the N^{por}−Fe−N^{por} axis. The energy level of the d_{xz} orbital differs from that of the d_{yz} orbital, so very different spin densities are found on porphyrin carbon atoms of the same type. However, the average values can still be related to the hyperfine shifts measured in solution, as shown in Table 1 and Figure 2. On the basis of the theoretical results, the ranges of C$^\alpha$, C$^\beta$, and C^{meso} chemical shifts for such a "frozen" conformation are about 50, 200, and 100 ppm, respectively. Since there is no splitting of the C$^\alpha$, C$^\beta$, or C^{meso} shifts seen experimentally,[52] this implies that the axial ligands must jump between N^{I}, N^{III} and N^{II}, N^{IV} orientations at a rate in excess of $\sim 10^5$ sec^{-1}, in solution, although at any given time they are aligned along one or the other N^{por}−Fe−N^{por} axes.

In addition to these results, we also evaluated the atomic spin (Mulliken) populations for $[Fe(TPP)(Im)_2]^+$. For the porphyrin C$^\alpha$, C$^\beta$, C^{meso}, and N^{por} atoms, the computed values for model 1 are as follows: 0.0051, 0.0103, −0.0050, and −0.0122 (BPW91); 0.0052, 0.0055, −0.0042, and −0.0194 (B3LYP). Similar results are obtained for model 2. Application of the Karplus and Fraenkel relationships to combined ^{13}C and ^{1}H NMR data can also be used to estimate the atomic spin population for porphyrin ring atoms, and values of 0.0055, 0.0120, −0.0015, and 0.0100 have been reported by Goff.[52] The only noticeable deviation is found for N^{por}, which may be due at least in part to the assumption in Goff's calculation that the empirical parameters for the polarization between the carbon and the nitrogen atoms are the same as those for the polarization between carbons atoms.

High-Spin Fe(III) ($S = {}^5/_2$) and Mn(III) ($S = 2$) Porphyrins. We have also investigated three five-coordinate high-spin Fe(III) and Mn(III) tetraphenylporphyrins: Fe(TPP)Cl, Mn(TPP)Cl, and Mn(TPP)Br. As can be seen from Table 1, although there is no particular ordering of the hyperfine shifts for the halide manganese porphyrin complexes, the following trends do exist: the hyperfine shifts for C$^\alpha$ are downfield (at about 245 ppm); the C$^\beta$ shifts are upfield (at about −290 ppm); and the C^{meso} signals exhibit small upfield shifts. The hyperfine shift pattern for the halide manganese complexes is significantly different from that for Fe(TPP)Cl, whose ^{13}C NMR spectrum exhibits pyrrole C$^\alpha$ and C$^\beta$ hyperfine shifts in the 1000−1200 ppm region.[46] The principal reason for this is that the metal atoms have different electronic configurations. For high-spin Fe(III), the d-orbital configuration is $(d_{xy})^1(d_{xz}d_{yz})^2(d_{z^2})^1(d_{x^2-y^2})^1$, while the orbital configuration is $(d_{xy})^1(d_{xz}d_{yz})^2(d_{z^2})^1(d_{x^2-y^2})^0$ for high-spin Mn(III). The $d_{x^2-y^2}$ orbital is singly occupied in Fe(TPP)Cl and vacant in Mn(TPP)Cl. This difference results in these two high-spin complexes having very different electronic structures and is reflected in their spin delocalization and hyperfine shift patterns.

In Fe(TPP)Cl, the porphyrin macrocycle is almost planar, exhibiting approximately D_{4h} symmetry. The iron atom is out-of-plane by about 0.528 Å, and the bond length between the iron and the porphyrin nitrogens is about 2.070 Å. In contrast, the porphyrin core of Mn(TPP)Cl is highly distorted, having a pronounced saddle geometry, which can best be described by C_{2v} symmetry. The Mn atom is displaced from the mean N^{por} plane by only 0.025 Å, and the Mn−N^{por} bonds are much shorter, about 2.008 Å. These structural differences can be explained to some extent by the occupation of the $d_{x^2-y^2}$ orbital in Fe(TPP)Cl, in which the lobes of the $d_{x^2-y^2}$ orbital are oriented toward the four N^{por} atoms. The singly occupied $d_{x^2-y^2}$ orbital in Fe(TPP)Cl increases the repulsion between the iron and the porphyrin nitrogens and results in the longer Fe−N^{por} bonds, together with an out-of-plane displacement of the iron atom. On the other hand, the missing repulsive interaction due to the vacant $d_{x^2-y^2}$ orbital in Mn(TPP)Cl enables Mn to be much closer to the porphyrin nitrogens. These relatively short Mn−N^{por} bonds thus contract the porphyrin core and favor the saddle distortion. Figure 8 shows contour plots of the frontier MOs for Fe(TPP)Cl and Mn(TPP)Cl. The HOMO of Fe(TPP)Cl (Figure 8A) is characterized by a strong σ interaction between the $d_{x^2-y^2}$ orbital and the nitrogen-based porphyrin orbital $b_{1g}(n)$. This strong σ-interaction is expected to contribute significantly to spin density delocalization. Since the $d_{x^2-y^2}$ orbital is vacant in Mn(TPP)Cl, the HOMO (Figure 8B) is formed by σ interaction between the highest singly occupied d_{z^2} orbital and the porphyrin HOMO orbital, both of which transform according to the same representation, a_1. This σ interaction is weak, however, because of a lack of sufficient orbital overlap, and it cannot make a significant contribution to the spin density delocalization. The unpaired spin density is primarily delocalized through the much stronger π interaction between the lower-energy π-symmetry orbitals, for example the metal d_{xz}/d_{yz} and the porphyrin $e_g(\pi)$ orbitals. Parts C and D of Figure 8 show contour plots of the two symmetric MOs formed by this kind of π interaction, for Mn(TPP)Cl. These results indicate that

(60) Walker, F. A.; Huynh, B. H.; Scheidt, W. R.; Osvath, S. R. *J. Am. Chem. Soc.* **1986**, *108*, 5288−5297.

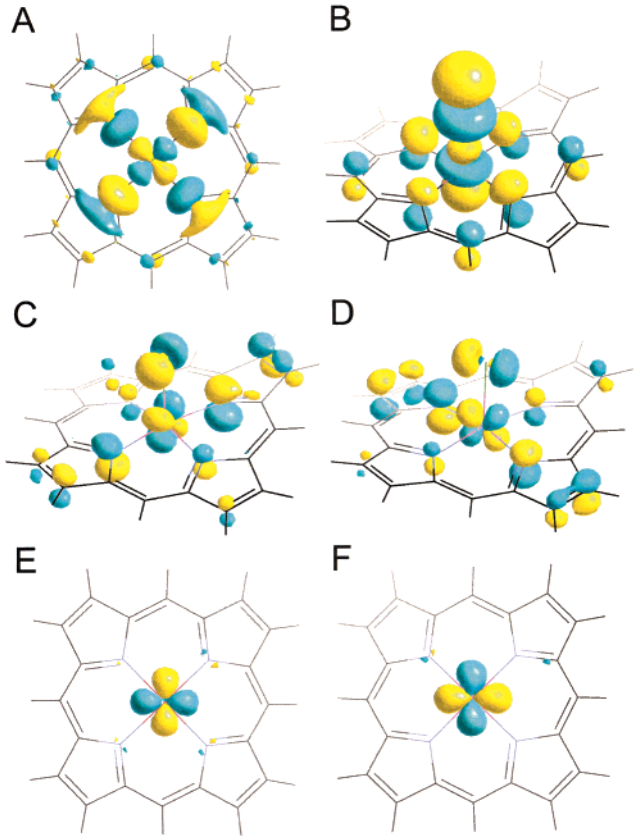

Figure 8. Isosurface representation of the frontier molecular orbitals (contour values = ±0.04 au) of (A) Fe(TPP)Cl, α-HOMO; (B) Mn(TPP)-Cl, α-HOMO; (C) Mn(TPP)Cl, α-HOMO-5; (D) Mn(TPP)Cl, α-HOMO-6; (E) Fe(TPP)Cl, d_{xy} MO; and (F) Mn(TPP)Cl, d_{xy} MO.

different spin density delocalization mechanisms are operative in these two complexes. For Fe(TPP)Cl, σ-spin delocalization dominates, while for Mn(TPP)Cl, π-spin delocalization dominates. These results are supported by the experimental hyperfine shift and computed spin density results. For example, for Fe(TPP)Cl, the spin densities on the pyrrole α and β carbon atoms are large and positive, corresponding to strongly downfield hyperfine shifted signals in the 1000−1200 ppm region.[46] This result is typical of the σ-spin delocalization via donation from the singly occupied σ-symmetry $d_{x^2-y^2}$ orbital.[61,62] As to the large downfield C^{meso} hyperfine shift, this can be related to π-spin delocalization, since the porphyrin $e_g(\pi^*)$ LUMO set has a large amplitude at the C^{meso} positions. This $(d_{xz}d_{yz})^2 \rightarrow e_g(\pi^*)$ back-bonding mechanism locates positive π-spin density on C^{meso}, resulting in a downfield shift. So, predominant σ-spin and complementary π-spin delocalization mechanisms are operative for the high-spin ferric Fe(TPP)Cl complex. For Mn(TPP)Cl, the computed spin densities for C^{α} and C^{β} are of opposite sign, consistent with the observation of downfield C^{α} and the upfield C^{β} hyperfine shifts. This pattern is associated with π-spin delocalization through the $e_g(\pi)$-like MOs. This MO pair exhibits nodes at C^{meso} and contributes little to the C^{meso} hyperfine shift. The rather small upfield shift of C^{meso} can be ascribed to polarization by the positive spin density on the neighboring C^{α} atoms. The metal d_{xy} orbital is usually regarded as a nonbonding orbital in such porphyrin complexes,[43,48] and we show in Figure 8E and F the two MOs containing the major metal d_{xy} component, for Fe(TPP)Cl and Mn(TPP)Cl, respectively. As expected, both MOs come solely from donation from the d_{xy} orbital. The unpaired electrons in both orbitals are localized on the metal atoms and make no major contributions to spin density delocalization onto the porphyrin macrocycles.

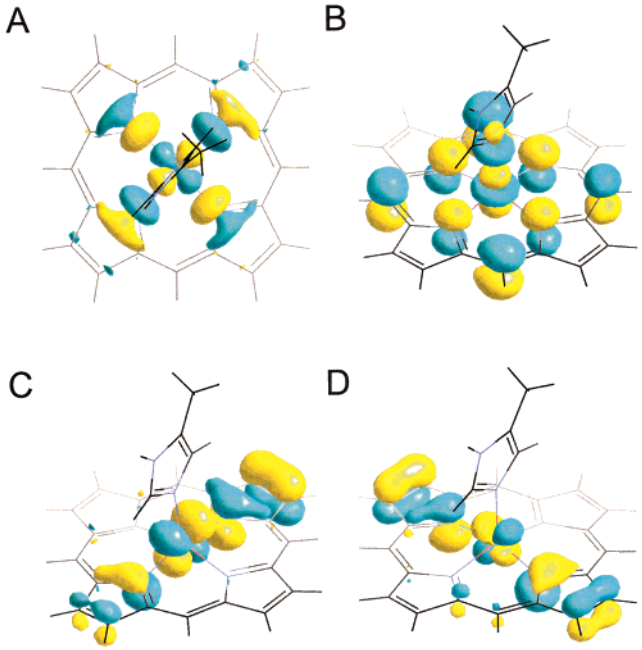

Figure 9. Isosurface representation of the frontier molecular orbitals of deoxyMb model system (based on PDB File # 1A6N, contour values = ±0.04 au): (A) α-HOMO; (B) α-HOMO-1; (C) α-HOMO-3; (D) α-HOMO-5.

High-Spin Fe(II) ($S = 2$) DeoxyMb. For high-spin Fe(II), the d-orbital configuration is $(d_{xy})^2(d_{xz}d_{yz})^2(d_{z^2})^1(d_{x^2-y^2})^1$. As noted above, the pyrrole C^{α} and C^{β} hyperfine shifts for the deoxyMb model compound are in the 650−900 ppm range. Such large downfield pyrrole carbon shifts are expected as a consequence of a strong σ interaction between the $d_{x^2-y^2}$ unpaired spin and the pyrrole nitrogen atoms (Figure 9A). Likewise, the downfield hyperfine shifts for the imidazole carbon atoms are likely due to the unpaired spin in the d_{z^2} orbital (Figure 9B). And finally, the close-to-zero C^{meso} hyperfine shift indicates the involvement of porphyrin $e_g(\pi)$ instead of $e_g(\pi^*)$ orbitals (Figure 9C and D).

^{13}CN Ligand Shifts in $[Fe(TPP)(CN)_2]^-$ and MbCN. Finally, after review of this paper, an interesting experimental paper appeared on ^{13}CN shifts in bis(cyanide) porphyrin complexes as well as in sperm whale (*Physeter catodon*) cyanometmyoglobin.[63] Since the wave function for the $[Fe(TPP)(CN)_2]^-$ model had already been computed, as had that for a *P. catodon* MbCN (unpublished results), we were interested to see to what extent these shifts were predictable theoretically. On the basis of our previous results, where we found the best accord between theory and experiment when using the B3LYP hybrid XC functional, it seemed likely that the best accord would also be obtained for the axial CN ligands using this functional. This is clearly the case. We show in Table 4 the computed $\rho_{\alpha\beta}$ values (B3LYP results) and the predicted shifts for these axial cyanide

(61) Goff, H. M.; Hansen, A. P. *Inorg. Chem.* **1984**, *23*, 321−326.
(62) Walker, F. A.; Simonis, U. In *Biological Magnetic Resonance*; Berliner, L. J., Reuben, J., Eds.; Plenum Press: New York, 1993; Vol. 12, pp 133−274.
(63) Fujii, H. *J. Am. Chem. Soc.* **2002**, *124*, 5936−5937.

Table 4. Experimental ^{13}CN NMR Shifts, Computed Fermi Contact Spin Densities, and Predicted Shifts in Cyanide-Bound Porphyrin Complexes ($S = {}^1/_2$)

system	structure model	δ_{obs}[a] (ppm)	δ_{hf}[b] (ppm)	δ_{con}[c] (ppm)	$\rho_{\alpha\beta}$ (au)	predicted δ_{con} (ppm)
K[Fe(PPDME)(CN)$_2$][d]	K[Fe(TPP)(CN)$_2$]	−2516	−2693	−3093	−0.02990	−2867
MbCN (sperm whale)	MbCN (sperm whale)	−4145	−4322	−4722	−0.05093	−4881

[a] Recorded at 296 K, ref 63. [b] δ_{hf} is obtained by subtracting the diamagnetic shift 177 ppm from the observed chemical shift. The diamagnetic reference is K$_4$[Fe(CN)$_6$], 299 K (see: Goff, H. *J. Am. Chem. Soc.* **1977**, *99*, 7723−7725). [c] $\delta_{con} = \delta_{hf} - \delta_{dip}$. The dipolar shift is estimated to be ∼400 ppm, ref 64. [d] PPDME: protoporphyrinIX dimethyl ester.

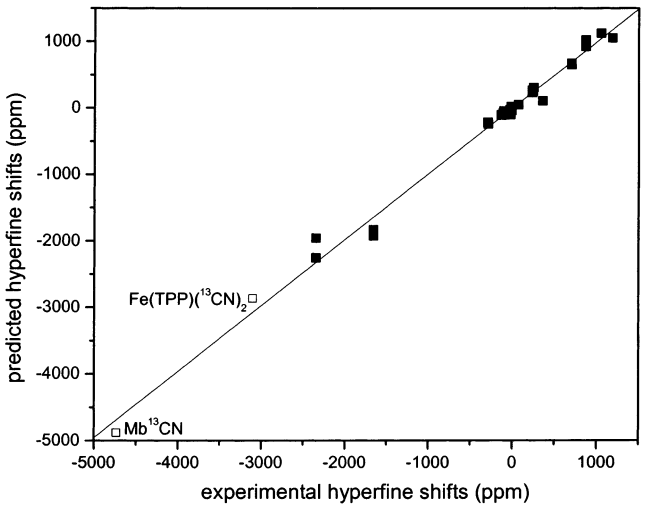

Figure 10. Graph showing experimental NMR hyperfine shifts over the entire ∼6000 ppm range plotted as a function of the hyperfine shifts computed by using the DFT/B3LYP method and eq 7. (■) represents data from Table 1, and (□), ^{13}CN contact shifts of a bis(cyanide) porphyrin complex and sperm whale cyanometmyoglobin from Table 4. The line is drawn through all 39 data points and has a slope of 0.99 and an R^2 value of 0.990.

ligands. Since the dipolar shifts are estimated to be ∼400 ppm,[64] which are not negligible, we use the contact shifts here to compare with the predictions. For the [Fe(TPP)(CN)$_2$]$^-$ model, we find a predicted −2867 ppm shift, to be compared with an estimated −3093 ppm experimental contact shift value, while for MbCN, we predict a shift of −4881 ppm, to be compared with a −4722 ppm experimental contact estimate, Table 4. These results are very interesting since they extend by ∼2500 ppm the overall shift range, which now covers 6000 ppm, Figure 10. The correlation line in Figure 10 has an $R^2 = 0.990$ ($N = 39$) and strongly suggests that quantum chemical methods will be of use in predicting the resonance positions of other metal-bound ligands in paramagnetic systems.

(64) La Mar, G. N.; Walker, F. A. In *The Porphyrins*; Dolphin, D., Ed.; Academic Press: New York, 1978; Vol. 3, pp 61−157.

Conclusions

The results we have described above are of interest for a number of reasons. First, we have carried out a series of density functional theory calculations of the electronic structures of a range of $S = {}^1/_2$, $S = 2$, and $S = {}^5/_2$ metalloporphyrins and related systems. The results yield information on the Fermi contact spin densities at ^{1}H, ^{13}C, ^{15}N, and ^{19}F sites, which are shown to be highly correlated with experimentally determined NMR hyperfine shifts. When the results of recent experimental ^{13}CN ligand shift determinations are included, the total experimental shift range is ∼6000 ppm and the theory versus experiment correlation is 0.990 ($N = 39$). Second, the theoretical results obtained have led to a reappraisal of some earlier measurements of ^{13}C NMR hyperfine shifts in the paramagnetic protein, deoxymyoglobin. The DFT results when combined with accurate integrated intensities lead to the conclusion that only the C$^\beta$ hyperfine shifted carbons are being detected in deoxymyoglobin, together with most likely those of C$_5$ and C$_2$ in the proximal histidine residue. Third, our results give detailed information on the spin density distributions in several $S = {}^1/_2$ systems. Fourth, our results give detailed pictures of the orbital interactions which lead to the experimentally observed hyperfine shifts. When taken together, the results described above indicate that DFT methods now enable the quite accurate prediction of many heavy atom shifts in metalloporphyrins and a metalloprotein. This ability to predict hyperfine shifts in highly conjugated systems can be expected to lead to more quantitative studies of the static and electronic structures of metalloporphyrins and metalloproteins by using the NMR hyperfine shift as a structure probe.

Acknowledgment. We thank G. Meints and C. Lea for obtaining the result shown in Figure 4. J. Mao was supported by an American Heart Association, Midwest Affiliate, Predoctoral Fellowship. This work was supported by the United States Public Health Service (NIH Grant EB 00271-24) and by the National Computational Science Alliance (Grants MCB-000018N, MCB-000020N, and MCB-010016N).

JA020297W